Shallow snow depth mapping with unmanned aerial systems lidar observations: A case study in Durham, New Hampshire, United States

Jennifer M. Jacobs[1,2], Adam G. Hunsaker[1,2], Franklin B. Sullivan[2], Michael Palace[2,3], Elizabeth A.
5 Burakowski[2], Christina Herrick[2], Eunsang Cho[1,2]

[1]Department of Civil and Environmental Engineering, University of New Hampshire, Durham, NH, 03824, USA
[2]Earth Systems Research Center, Institute for the Study of Earth, Oceans, and Space, University of New Hampshire,
Durham, NH, 03824, USA
[3]Department of Earth Sciences, University of New Hampshire, Durham, NH, 03824, USA

Correspondence to: Jennifer M. Jacobs (Jennifer.jacobs@unh.edu)

Abstract. Shallow snowpack conditions, which occur throughout the year in many regions as well as during accumulation and ablation periods in all regions, are important in water resources, agriculture, ecosystems, and winter recreation. Terrestrial and airborne (manned and unmanned) laser scanning and structure from motion (SfM) techniques have emerged

15 as viable methods to map snow depths. Lidar on an unmanned aerial vehicle is also a potential method to observe field and slope scale variations of shallow snowpacks. This paper describes an unmanned aerial lidar system, which uses commercially available components, for snow depth mapping on the landscape scale. The system was assessed in a mixed deciduous and coniferous forest and open field for a shallow snowpack (< 20 cm). The lidar ground point clouds yielded an average of 90 and 364 points/m^2 in the forest and field, respectively. Comparisons of snow probe and lidar mean snow

20 depths in the field, at 0.4 m resolution, had a mean absolute difference of 0.96 cm and a root mean squared difference of 1.22 cm. In the forest, the *in situ* mean snow depth was nearly twice that from the lidar from mean absolute difference of 9.6 cm and root mean squared difference of 10.5 cm. These differences in forests are likely due, in part, to limitations of sampling using a snow probe. At 1 m resolution, the field snow depth precision was consistently less than 1 cm. The forest and heavily vegetated areas had modestly reduced performance with typical values within 4 cm precision. Performance depends on both

25 the point cloud density, which can be increased or decreased by changing the flight plan, and the within cell variability that depends on site surface conditions.

1 Introduction

In many regions, shallow snowpacks, i.e., snow depth less than 20 cm, are typical throughout the winter. Even in mountainous regions with deep seasonal snowpacks, snowpacks can be shallow and nonuniform during the accumulation

30 and melt periods as well as in areas with high winds. Shallow snowpacks impact many hydrologic, agricultural, and

ecosystem processes. Shallow snowpack characteristics effect the location and condition of suitable habitats in animal populations (Friggens et al., 2018). Meltwaters from shallow snowpacks can be a major contributor to streamflow and spring floods in many regions (Tuttle et al., 2017) and intensify overland nutrient transport and soil erosion (Seyfried et al., 1990; Singh et al., 2009). Thin, ephemeral snowpacks allow the underlying soils to freeze more readily in the winter because they

35   lack the insulating properties of deeper packs and the shallower snow's higher albedo may increase deep-freezing (Starkloff et al. 2017). Soil frost severity impacts soil respiration, carbon sequestration, nutrient retention, and microbial communities as well as a plant root health and tree growth (Aase and Siddoway, 1979; Isard and Schaetzel, 1998; Monson et al., 2006; Henry, 2008; Aanderud et al., 2013; Tucker et al., 2016; Sorensen et al., 2018; Reinmann and Templer, 2018). When the frozen soils impede meltwater infiltration, flooding and erosion may increase (Watanabe and Osada, 2016). Winter

40   recreation is also affected by shallow snowpacks. In some regions, minimum snow depth restrictions for recreational activities are required (e.g., 30.5 cm for snowmobiling on US Forest Service lands) or being considered to reduce impacts to sensitive ecosystems (Hatchett and Eisen, 2019).

Shallow snowpacks are highly dynamic, accumulating and ablating throughout the winter with associated changes in

45   snowpack density, grain size, and albedo (Adolph et al., 2017) as well as ice formation. Wind redistribution, sloughing of snow off slopes, trapping of snow by vegetation, and forest canopy interception also result in a range of spatial features at varying scales (Clark et al., 2011; Mott et al., 2011; Mott et al., 2018). These variations cause shallow snowpacks to more readily ripen during winter rain events and warmer air temperature than deeper snowpacks (Wever et al., 2014) and, in combination with the transport and refreeze of meltwaters (Watanabe and Osada, 2016) make modeling and mapping of

50   shallow snowpacks extremely challenging (Hall et al., 2010; Gichamo and Tarboton 2019; Starkloff et al., 2017). Despite their prevalence, complexity, and importance, shallow snowpacks have received relatively little attention for measurement, modelling, and mapping efforts.

Because shallow snowpacks have considerable spatiotemporal variability, a large number of snow depth measurements are

55   often needed to characterize the snowpack (Dickinson and Whiteley, 1972). Using traditional point measurements with its limited sample size requires a balance between the sampling extent and sample spacing; this impacts the ability to capture spatial variability that naturally increases with spatial scale as compared to capturing small-scale spatial structures (Clark et al. 2011). Over the past two decades, airborne remote sensing methods, providing spatially continuous, high-resolution snow depth maps at local and regional scales, have greatly advanced the ability to characterize the spatiotemporal variability of

60   snow depth over earlier work using snow probes (see reviews in Deems et al., 2013; López-Moreno et al., 2017). Airborne laser scanning (ALS) (Deems et al., 2013; Harpold et al., 2014; Kirchner et al., 2014), terrestrial laser scanning (TLS) (Grünewald et al. 2010; Currier et al. 2019), and structure-from-motion photogrammetry (SfM) (Nolan et al., 2015; Bühler et al., 2016; Harder et al., 2016) have emerged as viable methods to map surface elevations with snow-off and snow-on conditions in order to differentially map snow depths.

65

ALS and TLS both rely on well-established lidar (light detection and ranging) technology. TLS, applied from a fixed ground position, is able to measure snow depth with high vertical accuracy (Fey et al., 2019), and has the advantage of being relatively low-cost and portable, making repeat observations possible. However, TLS uncertainties are caused by large incident angles, occlusion from hills and trees that can cause data gaps in forested domains (Currier et al., 2019; Palace et al.,

70   2016), and challenges providing a stable scanner position for the tripod in snow-on conditions (Schweizer et al., 2003). ALS technology such as that deployed on the Airborne Snow Observatory (ASO) (Painter et al., 2016) has the advantage of being able to cover large areas, but it is extremely expensive and has limited availability, which impacts its use for most studies. ALS also has issues with observation gaps in forested regions (Broxton et al., 2015; Currier and Lundquist, 2018; Mazzotti et al., 2019) but possibly to a lesser extent than TLS (Currier et al., 2019). For shallow snowpacks, the typical vertical

75   accuracies from these platforms, on the order of 10 cm (Kraus et al., 2011; Deems et al., 2013), as well as relatively low return density ($\sim$10 returns/m^2) (Cook et al., 2013) are not adequate to observe spatial variations from micro to field scales of shallow snowpacks.

SfM can create a digital surface model (DSM) from photographs taken using a standard consumer-grade digital camera.

80   When deployed on an unmanned aerial system (UAS) platform, SfM is a low cost method that has the capacity for routine snow depth monitoring (Adams et al., 2018; Bühler et al., 2016; De Michele et al., 2016; Harder et al., 2016; Vander Jagt et al., 2015). Reported accuracies range from 8 to 30 cm using UAS SfM (Adams et al., 2018; Bühler et al., 2016; Goetz and Brenning, 2019; Harder et al., 2016; Meyer and Skiles, 2019). The primary drawbacks of UAS SfM as compared to lidar for mapping snow depth are that the DSM needs to be georeferenced using ground control points (GCPs) with known

85   coordinates and may require significant manual steps (Tonkin et al., 2016; Meyer and Skiles, 2019), although new techniques are emerging that may reduce field data collection time (Gabrlik et al., 2019; Meyer and Skiles, 2019). Dense canopy or vegetation can reduce performance when snow compresses the vegetation relative to the snow-off imagery or when above-canopy vegetation is falsely interpreted to be the snow surface (Bühler et al., 2017; Cimoli et al., 2017; De Michele et al., 2016; Fernandes et al., 2018; Harder et al., 2016; Nolan et al., 2015). Canopy effects impact SfM snow

90   mapping capability in regions where shallow snowpacks are masked by dense forest canopies like the northeastern United States.

UAS-based lidar has been widely used in forest-related research (e.g. canopy height and forest change detection) (Wallace et al., 2012; 2014) and appears to offer the advantages of both the UAS SfM and lidar for snow depth mapping. A UAS

95   platform also eliminates many of the drawbacks that arise from ALS and TLS systems discussed earlier. However, to date there are few previous studies that estimate snow depth using UAS-based lidar (Vander jagt et al., 2013). The purpose of this paper is to assess the ability of a UAS platform to provide snow depth using a modest cost UAS-based lidar. The pilot study described here serves as a proof-of-concept for shallow snowpack dataset production in open terrain and forests in the

northeastern United States. The study highlights results from the 2019 winter season that provide insights as to the potential

100   for UAS lidar mapping of snow depth as well as details about the system, its deployment and operational challenges. We explore the capability of UAS through the comparison of contemporary field-based snow depth measurements collected in a landscape containing fields and forests.
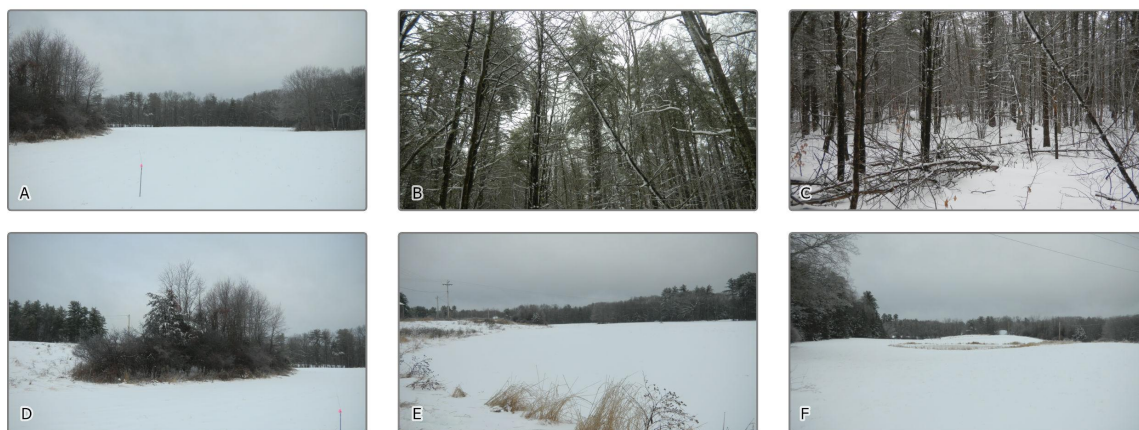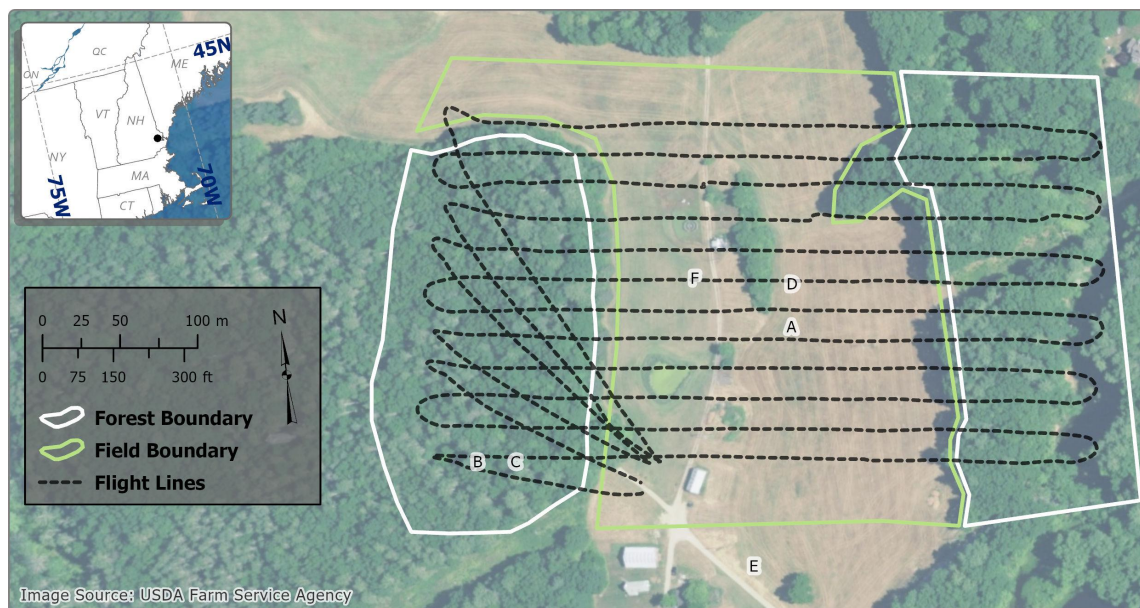
Figure 1. 2015 imagery of Thompson Farm, Durham NH showing both forest and field region with lidar flight lines (top). Ground imagery (a to f), collected in December 2019, locations are noted on the top map and show the surface and leaf off forest conditions (bottom panels).

2 Site, Data, and Methods

2.1 Site

110 The test flights were conducted at the University of New Hampshire Thompson Farm Research Station in southeast New Hampshire, United States (N 43.10892°, W 70.94853°, 35 m above sea level), which was chosen for its mixed hardwood forest and open field land covers (Burakowski et al., 2015; Burakowski et al., 2018) that are characteristic of the region (Figure 1). Thompson Farm has an area of 0.83 km^2 and little topographic relief (18 to 36 m ASL) (Perron et al., 2004). The agricultural fields are actively managed for pasture grass. The mixed deciduous and coniferous forest is composed primarily

115 of white pine (*Pinus strobus*), northern red oak (*Quercus rubra*), red maple (*Acer rubrum*), shagbark hickory (*Carya ovata*), and white oak (*Quercus alba*) (Perron et al., 2004). There are two "wood roads" that run north-south through the pasture and into the western forest section.

2.2 UAS Laser Scanning

A series of UAS lidar surveys were conducted over approximately a 0.1 km^2 (9.8 hectares) area (430 by 225 m) within the

120 farm during the winter 2018/2019 (Figure 1). Here, we focus on the snow-on flight conducted on January 23, 2019 and the snow-off flight conducted on April 11, 2019. We selected the January 23 flight because it had snowed approximately 11.5 cm with 1.8 cm of snow water equivalent from January 19th to January 20th and the air temperature was persistently below freezing prior to the flight. For the April 11, 2019 snow-off flight, the deciduous component of the canopy and understory were both dormant.

125

We used an Eagle X8 UAS manufactured by UAV America, which carried a small, light-weight (590 g) VLP-16 lidar (Velodyne, Inc.) suitable for UAS deployment. The VLP-16 is a 16-channel lidar with a 30-degree field of view with rotating lasers that are spaced evenly between -15 to +15 degrees, with each channel rotating 360-degrees. The VLP-16 collects up to 300,000 points per second with an accuracy of +/- 3 cm at a range of 100 m. Flights were conducted to

130 maximize spatial coverage while conserving batteries due to limited flight time with the Eagle X8 (approx. 9 minutes flight time to discharge to 3.6 V per cell). Automated flights were conducted using UgCS flight planning software. Because of the limited flight time, flights were conducted at an altitude of 81 m for greater spatial coverage and our flight plan included multiple return flight lines for the three battery exchanges (Figure 1). Our flight speed was 7 m/s, with a total of 12 parallel flight lines with targeted overlap of 40 percent. Because of degrading accuracy at distances >100 m with the VLP-16, returns

135 acquired outside of +/- 30 degrees of nadir view angles were filtered to limit target distance and improve overall accuracy.

The payload is equipped with an Applanix APX-15 UAV inertial navigation system (INS), which has 2-5 cm positional, 0.025-degree roll and pitch, and 0.08-degree true heading uncertainties following post-processing. The INS has a

measurement rate of 200 Hz, allowing for a timestamp to associate each lidar pulse with the closest data for latitude,
140 longitude, altitude, and perspective information (roll/pitch/yaw), which is required for georeferencing returns.

Data were post-processed to a Smoothed Best-Estimate Trajectory (SBET) file using POSPac MMS, resulting in approximately 3 cm positional accuracy for both the snow-on and snow-off flights. Lidar returns were matched to post-processed INS data and georeferenced using Headwall Photonics, Inc.'s Lidar Tools software. We performed boresighting
145 calibration using returns from the first two flight lines that were collected in antiparallel directions. Roll offset was determined using 10 m cross sections along the flight lines over flat terrain, and pitch offset was determined using 1 m cross sections across the flight lines over terrain with moderate relief. Resulting LAS point clouds were generated for the entire study area and projected in WGS84 UTM Zone 19N (EPSG 32619). Our flight and filtering parameters of the raw point cloud resulted in return densities of approximately 150 returns/m^2 for each of the two flights.

150 **2.3 Lidar Classification and Gridding**

Three-dimensional point clouds were classified as ground and non-ground points using the progressive morphological filter algorithm (PMF), in the lidR package (https://github.com/Jean-Romain/lidR) of R (v. 3.4, Team, 2018). The PMF operates iteratively on sets of two parameters, window size (w) and elevation thresholds (th) to erode and dilate point cloud data sets to estimate surface topography as a means to filter out non-ground returns from point cloud data sets (Zhang et al., 2003).
155 For ground classification, point clouds were chunked into 100 m square tiles with a 15 m buffer on all sides using catalog options in lidR to ensure returns near tile edges were classified. Processing was distributed across 8 computing cores to improve efficiency. We used a set of window sizes of 1, 3, 5, and 9 m, and elevation thresholds of 0.2, 1.5, 3, and 7 m, which were determined by varying value sets and assessing DTMs to determine the parameter sets that produced a visually smooth surface over a dense grid (*in sensu* Muir et al., 2017). Following processing, buffers were removed, and tiles were merged to
160 output final classified point clouds for each data set. Snow-on and snow-off ground point clouds were gridded at 0.1, 0.2, 0.4, 0.5, and 1.0 m spatial resolutions using the average of all grid points within each grid cell (Currier et al., 2019). Gridded products for each data set were forced to the same coordinate grid.

2.4 Snow Depth Ground Truth

A 1.2-m Global Positioning System (GPS)-equipped Magnaprobe (Sturm and Holmgren, 2018) was used to compare to the
165 unmanned aerial system (UAV) lidar surveys (hereafter noted as ALS measurements) over two transects. The first transect consisted of 12 sample locations in the field and 5 locations in the eastern forest of our study site. The second transect consisted of 11 sample locations in the western forest. Sample locations were separated by approximately 10 m. Each sample location includes 5 samples in a cross pattern with the four ordinal directions sampled approximately 20 cm from the center sampling location in the cross. Because the magnaprobe GPS has an absolute accuracy of 8 m, a Trimble© Geo7X
170 GNSS Positioning Unit with Zephr™ antenna was used to collect each sampling location's center point with an estimated

horizontal uncertainty of 2.51cm (standard deviation σ 0.95 cm) and 4.17cm (σ 4.60 cm) for the field and forest, respectively after differential correction. Along the same forest and field transects, a federal snow sampler was used to collect a single sample of snow depth and snow water equivalent at each location.

2.5 Snow Depth Uncertainty Assessment

175   The snow depth accuracy was assessed by comparing the lidar snow depth measurements to the magnaprobe measurements. Error statistics were calculated and the results were summarized by forest and field locations. At each magnaprobe location, the average and standard deviation of the five magnaprobe samples were calculated. The average lidar snow depth was determined for a 0.4 x 0.4 m cell centered on the center magnaprobe location. The mean absolute difference (MAD) and root mean square difference (RMSD) were used to characterize the differences between the magnaprobe snow depths and the
180   lidar snow depths.

The uncertainty of the lidar estimate of the snow depth mean value was calculated for each cell as the one-sided 95% confidence interval of the snow depth. A cell's snow depth pooled standard deviation σ_d of the snow on and snow off elevations was calculated as

185    $$\sigma_d = \sqrt{\sigma_{on}^2 + \sigma_{off}^2} \qquad (1)$$

where σ_{on} and σ_{off} are the standard deviation of the snow-on and snow-off lidar return elevations, respectively. The snow depth uncertainty was combined with the number of lidar returns and the pooled degrees of freedom (Helsel and Hirsh, 1992) to calculate the one-sided width of the 95% confidence limits for each cell.

3 Results and discussion

190   **3.1 Snow Depth Survey**

The snow-on and snow-off flights lidar ground returns yielded an average point cloud density of 90 and 364 points/m^2 in the forest and field, respectively, with 6.7% of the forest and 0.03% of the field cells having less than 5 point/m^2 (Figure 2). There is a wide range of the point cloud densities (Figure 2b). The highest point cloud density occurred for those cells sampled by both the regular flight lines and the multiple return flight lines conducted for the three battery exchanges. The
195   vast majority of field cells (82%) have more than 100 points/m^2. Only 1% of the field cells had less than 25 points/m^2 and most of those cells were in shrubbery or dense vegetation surrounding the small water body. In contrast, 41% of the forest cells had more than 100 points/m^2 and nearly 20% of the forest cells had less than 25 points/m^2 with 8% having fewer than 10 points/m^2 (Figure 2b). Only 0.086% and 0.95% of the 1 m resolution field and forest cells, respectively, had no ground returns. The number of points per cell decreases with decreasing the cell size (Figure 2a). In the field, reducing the gridded
200   resolution from 1 m to 0.5 m lowers the mean cell return count to 91 points per cell on average. Thus a 0.5 m field cell has

approximately the same number of returns as a 1 m forest cell. At a 0.2 m spatial resolution, the mean number of ground returns is 14.6 and 3.6 in the field and forest, respectively.
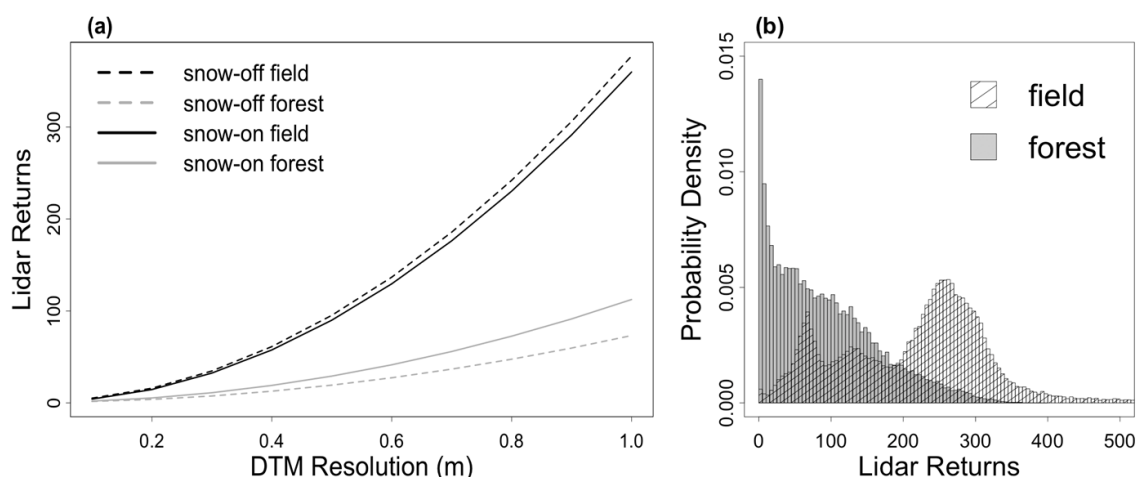
Figure 2. (a) Average lidar point cloud density of the ground returns with versus cell size by land cover, and snow-on and snow-off state (top). (b) Probability density function for the lidar ground returns point cloud density for 1 m^2 cell for the forest (gray) and the field (hashed) (bottom).

3.2 Snow Depth

Based on the magnaprobe snow depth and UAS-mapped snow depth measurements, the accuracy of lidar snow depth measurements differed between field and forest cells (Figure 3). In the field, the mean snow depth from the magnaprobe (12.2 cm ±0.56 cm) was only slightly greater than that from the lidar (11.2 cm ± 0.72 cm) and the MAD and RMSD values were 0.96 cm and 1.22 cm, respectively. In the forest, the mean snow depth from the magnaprobe (15.2 cm ± 2.3 cm) was twice as large as the lidar snow depths (7.8 cm± 6.3) and the MAD and RMSD were 9.6 cm and 10.5 cm, respectively. The mean snow depth from the snow tube was (12.9 cm ±0.71 cm) and (13.1 cm ±1.9 cm) in the field and forest, respectively. There is a notable low bias in the lidar forest snow depth relative to the magnaprobe and snow tube for west forest in particular with exception of one site.

3.3 Snow Depth Maps

The UAS-mapped snow depth, mapped by subtracting snow-off DTMs from snow-on DTMs, reveals a shallow snowpack whose depth ranges from less than 2 cm to over 18 cm (Figure 4). The mean snow depth was 10.3 cm in the field and 6.0 cm

in the forest. Despite the shallow conditions, spatially coherent patterns are readily discernible. The field snowpack depth has higher spatial variability than the west forest snowpack and more spatial organization. In the field, the deepest snow is in the
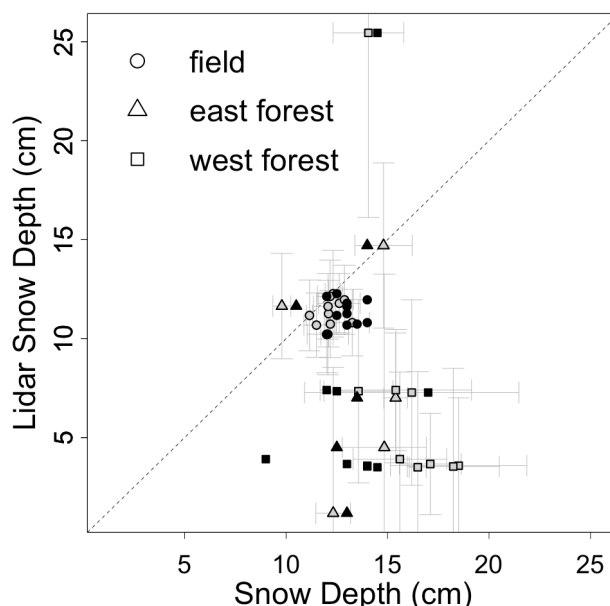
Figure 3. Comparison between the magnaprobe (gray fill) and snow tube (black fill) versus the lidar snow depth measurements by location. The mean and 95% confidence intervals were calculated using the five magnaprobe snow depths and the lidar snow depths averaged over a 0.4 x 0.4 m grid cell. The single snow tube snow depth measurement is shown without confidence intervals.

low-lying northeast areas that are sheltered from westerly winds. A relatively moderate and consistent snowpack occurs in southern part of the east field and west of the small pond. The shallowest snowpack is found in the center portion of the field, which is slightly elevated and, unlike most of the field, was not mowed. Lower snow depth at the forest edge distinguishes the field to forest transition. In the field, the precision of the mean snow depth estimate is remarkably consistent with one-sided confidence interval values typically between 0.5 to 1 cm regardless of snow depth (Figure 4). Modestly higher intervals occur adjacent to the north-south road where the fields were not mowed prior to winter as well as the northern and southern extents of the flight lines due to the reduced sampling density. The average one-sided confidence interval is considerably higher in the forest (3.5 cm) than the field. Where the forest is predominantly comprised of deciduous trees, the typical one-sided confidence interval of the mean snow depth is 1 to 2 cm. The largest one-sided confidence interval values occur in the middle of the field where there is dense shrubbery, at the edge of the fields, and in clusters within the forest where the forest sections are dominated by coniferous trees.

240
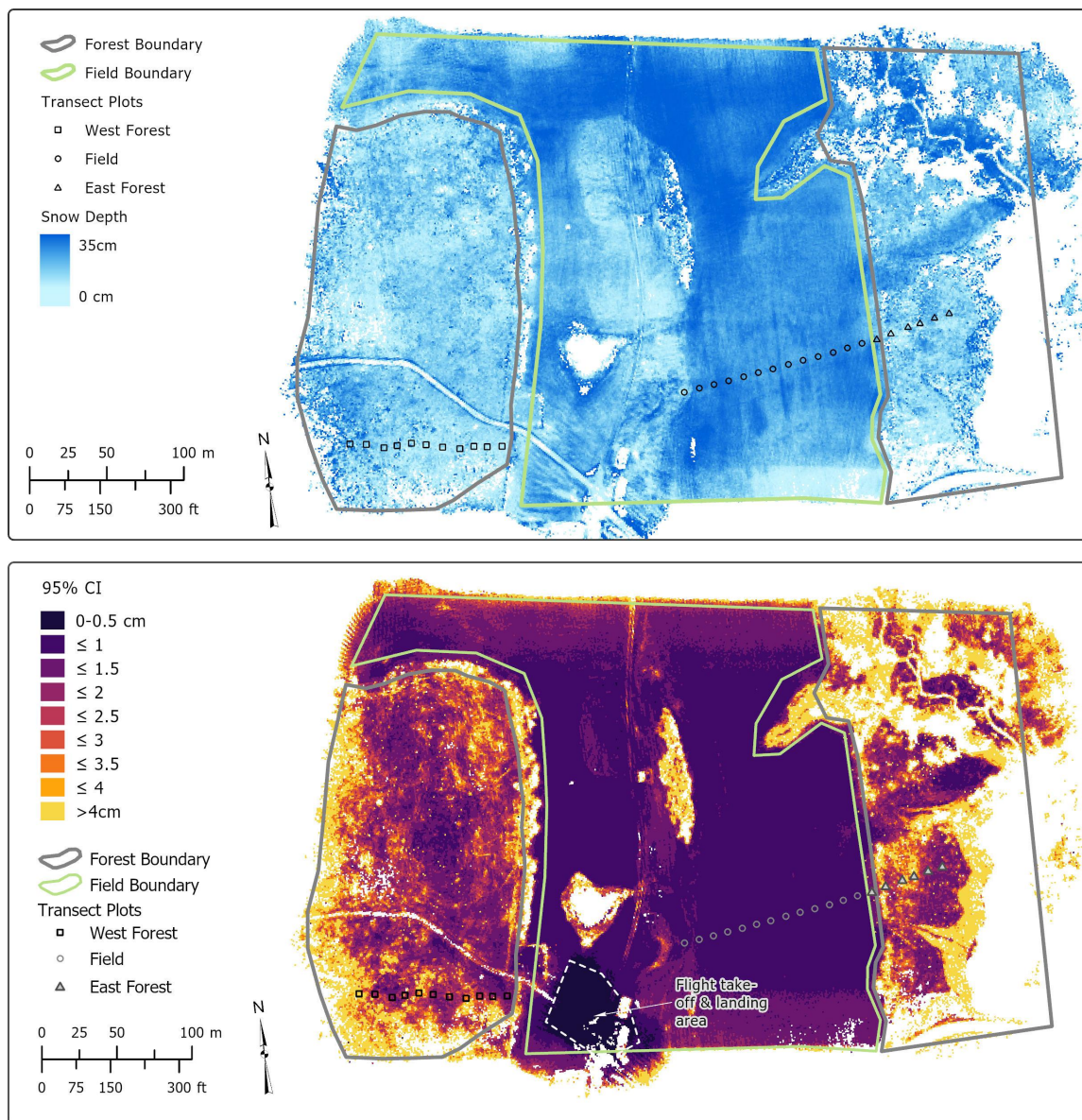
Figure 4. Average snow depth values (top) and one sided confidence intervals (bottom) calculated from the snow-on and snow-off lidar point clouds for 1 m^2 cells at Thompson Farm, Durham, NH on January 23, 2019.

3.4 Point Cloud Density and Spatial Resolution

245   Snow depth precision was examined in light of the point cloud density and the spatial resolution at which lidar returns were aggregated. The ability to precisely estimate mean snow depth of a 1 m^2 area increases dramatically as the lidar point cloud density increases (Figure 5a). Except for the cells with fewer than 10 point/m^2, forest cells have less precise estimates of the mean depths than field cells for a given sample size. When the density exceeds 25 point/m^2 in the field and 50 point/m^2 in the forest, precision is typically 2 cm. The cells with the highest point cloud densities have one-sided confidence intervals of

250   about 1 and 1.5 cm for the field and forest cells, respectively. The field cells with more than 50 point/m^2 did not have noticeably smaller confidence intervals, but the increased density did reduce the number of cells with anomalously low precision. Given the high lidar point cloud density for the field cells, it is possible that reasonably precise estimates of snow depth can be made at scales finer than 1 m (Figure 5b).

255
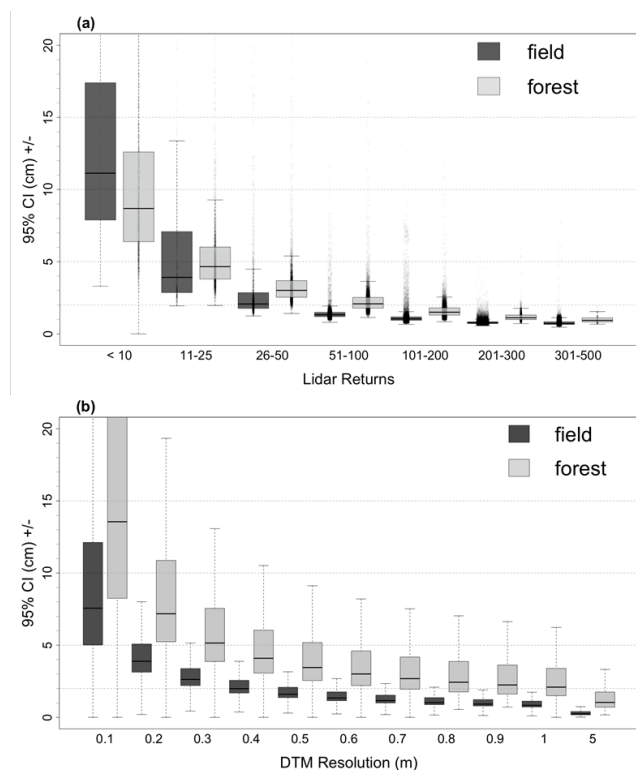
Figure 5. One sided confidence intervals of the mean snow depth values in the field and forest at Thompson Farm, Durham, NH on January 23, 2019 from the individual cells for 1 m2 cells by land cover and point cloud density (top) and for grid resolutions ranging 0.1 to 5 m (bottom). Boxplots show the lower quartile, median, upper quartile, and whiskers.

260 In addition to the lidar point cloud density, the ability to precisely capture the snow depth also depends on the within cell variability. For this site and its shallow snowpack, the local scale variability of the ground surface elevation was estimated by calculating the standard deviation of the lidar elevation values and found to depend primarily on the cell size and, to a more limited extent, on land cover and snow cover (Figure 6a). Within the 1 m grid cells, snow depth variability was much lower in the field than the forest (Figure 6b). Both distributions had a positive skew. Typical standard deviations of the lidar

265 surface elevation values within a 10 cm cell are on the order of 1.5 and 2 cm for the field and forest, respectively. That variability doubles for a 20 cm cell. The within cell variability increases gradually to about 3 to 4 cm in the field, and to about 6 cm in the forest. Snow cover reduces the within cell variability in field cells by about 1 cm, but has limited effect in the forest.

270 Thus, precision largely depends on the point per cell in the lidar cloud because the standard deviation of a cell's surface elevation is relatively constant for spatial scales from 0.5 to 1 m (Figure 6a). In the field, reducing the cell size from 1 m to 0.5 m still yields about 100 points/m^2 and provides snow depth estimates within +/- 1.5 cm. Because the forest cells require a higher ground return density to capture these snow depths within a 1 cm precision, any reduction in cell size below 1 m greatly decreases the precision of the cell mean snow depth.

275
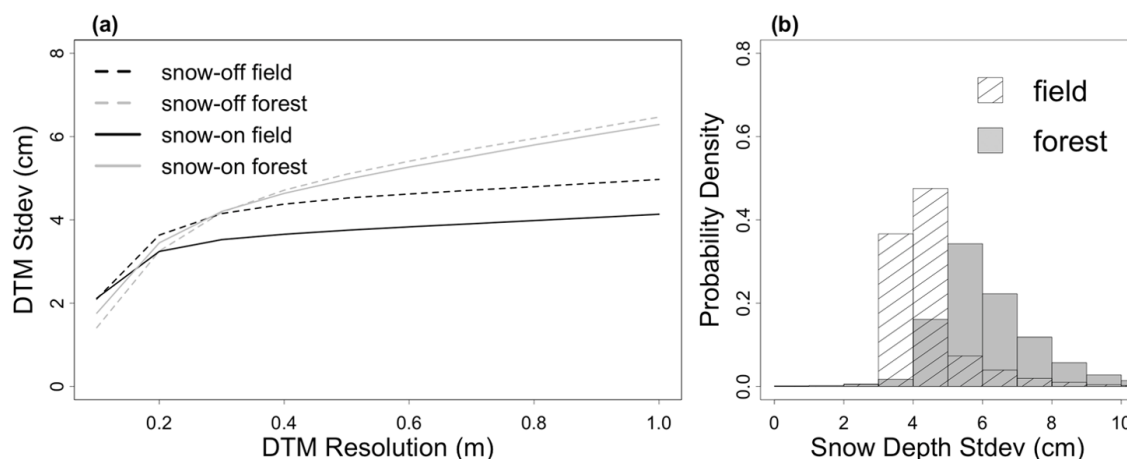
Figure 6. Lidar surface elevation standard deviations by cell size and land cover (top). (b) Probability density function of the pooled snow depth standard deviation for each 1 m^2 cell in the forest (gray) and field (hashed) (bottom).

280 **4. Challenges and Recommended Improvements to UAS Lidar Snow Depth Mapping**

Despite UAS-based lidar's increasing use in the natural sciences and capacity to make high resolution snow maps, there are many operational and technical challenges that require consideration prior to successfully conducting UAS-based lidar surveys that produce research grade data for snow hydrology. Large UAVs and supporting software analysis tools can be expensive and require trained pilots and lidar data analysis specialists. In this section, we present some preliminary insights

285 regarding the deployment of a lidar sensor on a UAV for snow depth mapping.

Because larger UAVs that can carry heavier payloads have challenges that may differ from small UAVs, a well-formulated flight plan is critical. Flight planning should address weather conditions, logistics of flying at proposed site, flight lines, UAS equipment, and personnel. Protocols should be developed and used consistently for each step of flight planning. Weather

290 conditions influence the safety and success of a UAS survey. UAS should not be operated when there is any type of precipitation or in dense fog/clouds. Moisture can cause electronic components to malfunction. Moisture build-up on the propellers can also adversely affect lift production. This project's Eagle X8 high lift capacity UAS cannot be flown comfortably in winds greater than 7.8 m/s. High wind speeds can also significantly reduce battery life as well as impact the accuracy of sensor observations. Cold air temperatures can cause batteries to rapidly discharge. For winter UAS surveys, all

295 flight and operational batteries should be kept warm prior to the UAS survey. This also applies to the computer used to upload flight lines and relay telemetry information. A MIL-STD-810 certified Panasonic Toughbook was used in this study to handle the anticipated cold temperatures. Additionally, cold temperatures can severely limit the dexterity of the person manipulating the flight controls. Proper gloves/clothing are required to effectively operate the flight controls in cold weather.

300 High lift UAVs capable of carrying a lidar sensor package have the potential to cause significant damage to person and property. The selection of a survey site not only needs to meet the objectives of the UAV survey, but also must have the proper attributes for safe and legal UAV operation. It is important that permission to operate the UAV at the site has been granted and that the land owner/public is aware of the UAV survey operations. Visual line of sight (VLOS) of the UAV needs to be maintained throughout the flight. It can be difficult to maintain VLOS while flying over forested or mountainous

305 sites. Spotters can be used if there is constant two-way communication between the spotters and the person operating the flight controls. For this study, an on-site, walk up tower allowed a spotter to maintain VLOS while the UAV was flown over the forest. Two-way communication was maintained throughout the flight.

In the first season, the project team experienced more than one situation that required the pilot to manually land the UAV.

310 Flying using first person view (FPV) by an experienced pilot is highly recommended for a UAS platform that is capable of handling large payloads such as this study's VLP-16 lidar. If an emergency occurs and the UAS needs to land as quickly as possible, FPV will help the pilot to orientate the UAV, safely land, and limit damage to the payload. For this study, the UAV

was equipped with low quality linearly polarized FPV antennas. The FPV signal was easily lost as the orientation of the drone relative to the base station changed. The FPV signal was also not able to penetrate the forest. Circular polarized FPV antennas are generally recommended for drones because they are not affected by transmitter/receiver orientation changes and are better at avoiding obstacle interference.

The deployment of a lidar system mounted on a UAV platform for snow depth monitoring requires flight patterns designed for bore sighting alignment and post-processing to ensure that point clouds are aligned (Painter et al., 2016). Provided that GNSS data are accurate, the most common reason for misalignment of point clouds is boresight angle errors (Li et al., 2019). Traditionally, boresighting calibration is performed using antiparallel flight lines and a perpendicular flight line to calculate IMU offsets (Keyetieu and Seube, 2019). Due to battery flight time limitations, we were unable to complete the flight pattern that is commonly used for boresighting alignment. Because of this, we leveraged our first two antiparallel flight lines for boresighting calibration. To determine roll offset, we used broad (10 m) along-path cross-sections over flat terrain, and to determine pitch offset we used narrow (1 m) across-path cross-sections in sloped terrain where the point clouds overlapped (Figure 7). Though not shown here, we additionally leveraged unique features within our data acquisition region, including barn roofs and deciduous tree branches to assess the resulting boresight angles (Kumari et al., 2011; Li et al., 2005). For this particular study, we performed boresight calibration manually. Methods often require extensive user input (Li et al., 2005), however boresight calibration is an increasingly automated process with wide variation in algorithms and approaches (e.g. Maas, 2000; Kumari et al., 2011; Zhang et al., 2019). In future work, we plan to explore automated boresight calibration methods to improve the accuracy of point cloud data sets.

While lidar calibration and data post-processing requirements are quite similar for UAS and airborne surveys, lidar surveys by the UAS platform deployed in this study have key differences from previous ALS surveys. A limitation noted above is that the UAS flight duration is considerably shorter causing the spatial extent to be much more limited than previous ALS snow depth surveys. An advantage is that the UAS's average point cloud density is much higher and has fewer missing pixels in the forest than previous ALS surveys. This study had ground returns of 90 and 364 points/m^2 in the forest and field, respectively, and had no ground returns in only 0.086% and 0.95% of the 1 m resolution field and forest cells, respectively. In contrast, ALS surveys typically report surface model densities between 8 to 16 points/m^2 (Broxton et al., 2015; 2019; Currier et al., 2019; Kirchner et al., 2014) and ground returns between 3 and 6 points/m^2 (Broxton et al., 2019; Kirchner et al., 2014). ALS derived snow depth maps have a much greater proportion of areas that are masked due to no ground returns, particularly under trees, with masking areas ranging from less to 10% to more than 23% (Harpold et al., 2014; Mazzotti et al., 2019). While gap filling is possible, interpolation using measured snow depth values to fill under tree can overestimate snow depth (Zheng et al., 2016).

345
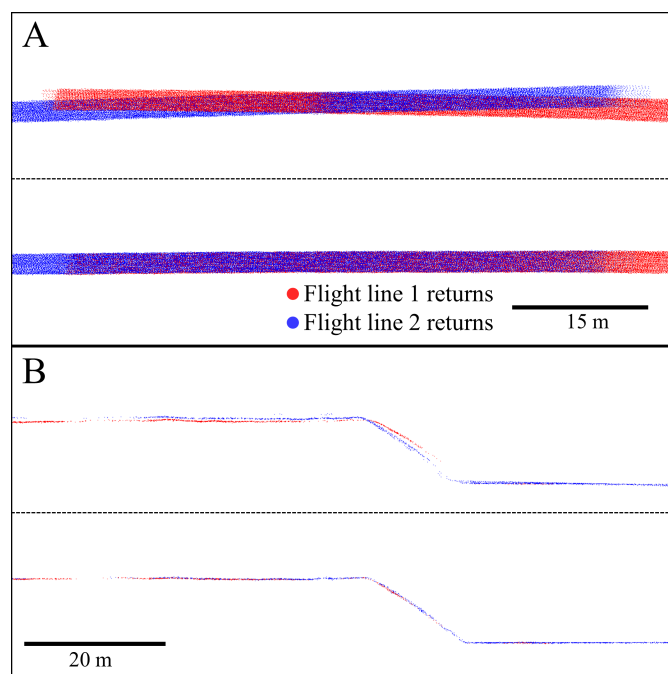
Figure 7. Uncalibrated boresight angles between the INS and lidar sensor can result in poorly aligned point clouds (A top and B top). Roll offsets present as crossed planes of data acquired from anti-parallel flight lines and are most clearly observed over flat terrain (A), while pitch offsets typically present as crossed planes of data acquired from perpendicular flight lines. Following boresight calibration, point clouds aligned well in both directions (A bottom and B bottom).

350

While UAS-based lidar surveys can measure snow depth to within a centimeter at high spatial resolutions, validation of those observations is challenging. A time consuming collection of high accuracy GNSS survey points was required to co-locate magnaprobe and lidar observations. Surveying in sample locations prior to the winter season might reduce this effort. It is also challenging to make *in situ* snow depth measurements that provide centimeter accuracy. In this study, the

355 magnaprobe *in situ* snow depth observations made in the forest were considerably higher than the lidar observations as compared to the open field where the magnaprobe and lidar measurements were within 1 cm. Previous studies also found that snow depth observations from ALS measurements are biased lower than those from snow-probe observations in the forest (Currier et al., 2019; Hopkinson et al., 2004). The cause of these differences is attributed to the snow probe's ability to penetrate the soil and vegetation, human observers tending to make snow depth measurements in locations with relatively

360 high snow (Sturm and Holmgren, 2018) and the reduced accuracy of the GNSS. Sturm and Holmgren (2018) indicate "The degree of penetration below the snow base is highly dependent on the nature of ground. For snow over sea, lake, or river ice, penetration is virtually zero and recorded depths are accurate to better than +0.1 cm. Over hard soils, rocks, and vegetation wetted in the fall and then frozen, the depth accuracy is nearly as high." In this study, the cold temperatures and no snow

365 conditions prior to the January 19th and 20th snowfall event resulted in deeper frozen soils (23.5 to 25.5 cm) in the field and thinner soil frost layers (5.5 to 8.5 cm) in the west forest, which would have limited the probe penetration into soils at both sites. However, the forest has a 1-4 cm thick loose leaf litter layer that may have been penetrated by the magnaprobe. The snow tube depths were not as deep as the magna probe and more closely match the lidar snow depth, further supporting that "over-probe" by the magnaprobe is responsible for the forest snow depth differences. A simple penetration test under similar snow depth and soil frost conditions revealed that the probe penetration into soil and leaf litter ranged from 0 to 10 cm,

370 averaging 5 cm over-probe bias over ten sample locations in the forest.

5. Conclusions

This paper describes and demonstrates a UAV lidar system for snow depth mapping using commercially available components. The UAS was assessed in a mixed deciduous and coniferous forest and open field with little relief. The UAS includes an Eagle X8 UAV manufactured by UAV America, a small, light-weight (590 g) VLP-16 lidar (Velodyne, Inc.),

375 and an Applanix APX-15 UAV inertial navigation system (INS). The INS has a measurement rate of 200 Hz, allowing returns to be georeferenced without additional ground control points. Data, post-processed to a Smoothed Best-Estimate Trajectory (SBET) file, resulted in approximately 3 cm positional accuracy. Flights were conducted at an altitude of 81 m and flight speed of 7 m/s, with a total of 12 parallel flight lines with targeted overlap of 40 percent. Once the point clouds were classified as ground and non-ground points, the flights yielded an average of 90 and 364 ground points/m^2 in a forest

380 canopy and field, respectively, with 6.7% of the forest and 0.03% of the field cells having less than 5 point/m^2.

The snow depth map, generated by subtracting snow-off from snow-on DTMs derived from the resultant point clouds, reveals a shallow snowpack whose depth ranges from less than 2 cm to over 18 cm. For 0.4 x 0.4 m cells, the *in situ* and lidar mean snow depths in the field were nearly identical with the MAD and RMSD values of approximately 1 cm. In the forest,

385 the *in situ* mean snow depths from a magnaprobe were twice as large as the lidar snow depths with a correspondingly high RMSD. These forest differences, which appear to be caused by the snow probe's ability to penetrate the soil and vegetation resulting in random errors, support previous findings indicating that there are limits to lidar snow depth validation at high horizontal and vertical spatial resolutions in some land covers and conditions. Mapped at 1 m^2 cells, a 0.5 to 1 cm snow depth precision was achieved consistently in the field with modestly reduced accuracy in the forest and heavily vegetated

390 areas. In the field, snow depth can be mapped at finer spatial resolutions with limited reduction in performance when reducing the cell size to 0.5 x 0.5 m and still achieving snow depth precision of less than 5 cm for a 0.2 x 0.2 m. Performance depends on both the point cloud density, which can be increased or decreased by changing the flight plan, and the within cell variability that depends on site surface conditions.

Acknowledgements

395 This material is based upon work supported by the Broad Agency Announcement Program and the Cold Regions Research and Engineering Laboratory (ERDC-CRREL) under contract number W913E5-18-C-005. Any opinions, findings and conclusions or recommendations in this material are those of the author(s) and do not necessarily reflect the views of the Broad Agency Announcement Program and the Cold Regions Research and Engineering Laboratory.

400 The authors are grateful to Lee Friess for providing a technical review of the draft manuscript, Mahsa Moradi Khaneghahi for supporting manuscript preparation, and Ronny Schroeder contributing to the field data collection.

Data Availability

The UAS-based lidar point clouds and in-situ snow observations are available from the corresponding author upon reasonable request.

405 **Author Contributions**

JJ, AH, FS, and MP designed research and performed analysis. JJ, AH, FS, MP, EB, and EC conducted field work to obtain lidar and/or in-situ snow observations. AH, FS, CH, and EC produced figures. JJ wrote the initial draft. All authors contributed to manuscript review and editing.

Competing Interests

410 The authors declare that they have no conflict of interest.

References

Aanderud, Z. T., Jones, S. E., Schoolmaster Jr, D. R., Fierer, N., and Lennon, J. T.: Sensitivity of soil respiration and microbial communities to altered snowfall. Soil Biol., 57, 217-227, 2013.

Adams, M. S., Bühler, Y. and Fromm, R.: Multitemporal accuracy and precision assessment of unmanned aerial system
415 photogrammetry for slope-scale snow depth maps in Alpine terrain. Pure Appl. Geophys., 175, 3303-3324, 2018.

Adolph, A. C., Albert, M. R., Lazarcik, J., Dibb, J. E. Amante, J. M. and Price, A.: Dominance of grain size impacts on seasonal snow albedo at open sites in New Hampshire. J. Geophys. Res.-Atmos., 122, 121-139, 2017.

Broxton, P., Harpold, A., Biederman, J., Troch, P. A., Molotch, N., and Brooks, P.: Quantifying the effects of vegetation structure on snow accumulation and ablation in mixed conifer forests. Ecohydrol., 8, 1073-1094. 2015.

420 Broxton, P. D., van Leeuwen, W. J., and Biederman, J. A.: Improving snow water equivalent maps with machine learning of snow survey and lidar measurements. Water Resour. Res., 55(5), 3739-3757, 2019.

Bühler, Y., Adams, M. S., Bösch, R., and Stoffel, A.: Mapping snow depth in alpine terrain with unmanned aerial systems (UASs): potential and limitations. The Cryosphere, 10, 1075-1088, 2016.

425 Bühler, Y., Adams, M. S., Stoffel, A., and Boesch, R.: Photogrammetric reconstruction of homogenous snow surfaces in alpine terrain applying near-infrared UAS imagery. Int. J. Remote Sens., 38, 3135-3158, 2017.

Cimoli, E., Marcer, M., Vandecrux, B., Bøggild, C. E., Williams, G., and Simonsen, S. B.: Application of low-cost UASs and digital photogrammetry for high-resolution snow depth mapping in the Arctic. Remote Sens., 1144, 2017.

Clark, M. P., and Coauthors: Representing spatial variability of snow water equivalent in hydrologic and land-surface models: A review. Water Resour. Res., 47. 2011.

430 Cook, B. D., and Coauthors: NASA Goddard's LiDAR, Hyperspectral and Thermal (G-LiHT) Airborne Imager. Remote Sens., 5, 4045-4066, 2013.

Currier, W. R., and Lundquist, J. D.: Snow depth variability at the forest edge in multiple climates in the western United States. Water Resour. Res., 54, 8756-8773, 2018.

Currier, W.R., Pflug, J., Mazzotti, G., Jonas, T., Deems, J.S., Bormann, K.J., Painter, T.H., Hiemstra, C.A., Gelvin, A.,
435 Uhlmann, Z. and Spaete, L.: Comparing aerial lidar observations with terrestrial lidar and snow-probe transects from NASA's 2017 SnowEx campaign. Water Resour. Res., 55(7), 6285-6294, 2019.

De Michele, C., and Coauthors: Using a fixed-wing UAS to map snow depth distribution: an evaluation at peak accumulation. The Cryosphere, 10, 511–522, doi:10.5194/tc-10-511-2016, 2016.

Deems, J. S., Painter, T. H. and Finnegan, D. C.: Lidar measurement of snow depth: a review. J. Glaciol., 59, 467-479.

440 Dickinson, W., and Whiteley, H.: A sampling scheme for shallow snowpacks. Hydrol. Sci. J., 17, 247-258, 2013.

Fernandes, R., and Coauthors: Monitoring snow depth change across a range of landscapes with ephemeral snowpacks using structure from motion applied to lightweight unmanned aerial vehicle videos. The Cryosphere, 12, 3535-3550, 2018.

Fey, C., Schattan, P., Helfricht, K., and Schöber, J.: A compilation of multitemporal TLS snow depth distribution maps at the
445 Weisssee snow research site (Kaunertal, Austria). Water Resour. Res., 55(6), 5154-5164, 2019.

Friggens, M. M., Williams, M. I., Bagne, K. E., Wixom, T. T., and Cushman, S. A.: Effects of climate change on terrestrial animals [Chapter 9]. In: Halofsky, Jessica E.; Peterson, David L.; Ho, Joanne J.; Little, Natalie, J.; Joyce, Linda A., eds. Climate change vulnerability and adaptation in the Intermountain Region [Part 2]. Gen. Tech. Rep. RMRS-GTR-375. Fort Collins, CO: US Department of Agriculture, Forest Service, Rocky Mountain Research Station. 375,
450 264-315, 2018.

Hatchett, B. J., and Eisen, H. G.: Brief Communication: Early season snowpack loss and implications for oversnow vehicle recreation travel planning. The Cryosphere, 13, 21-28, 2019.

Gabrlik, P., Janata, P., Zalud, L., and Harcarik, J.: Towards automatic uas-based snow-field monitoring for microclimate research. Sensors, 19(8), 1945, 2019.

455 Gichamo, T. Z., and Tarboton, D. G.: Ensemble streamflow forecasting using an energy balance snowmelt model coupled to a distributed hydrologic model with assimilation of snow and streamflow observations. Water Resour. Res., 55(12), 10813-10838, 2019.

Goetz, J., and Brenning, A.: Quantifying uncertainties in snow depth mapping from structure from motion photogrammetry in an alpine area. Water Resour. Res., 55, 7772-7783, 2019.

460 Grünewald, T., Schirmer, M., Mott, R., and Lehning, M.: Spatial and temporal variability of snow depth and SWE in a small mountain catchment. The Cryosphere, 4, 215-225, 2010.

Hall, D. K., Riggs, G. A., Foster, J. L., and Kumar, S. V.: Development and evaluation of a cloud-gap-filled MODIS daily snow-cover product. Remote Sens. Environ., 114(3), 496-503. 2010.

Harder, P., Schirmer, M., Pomeroy, J. and Helgason, W.: Accuracy of snow depth estimation in mountain and prairie
465 environments by an unmanned aerial vehicle. The Cryosphere, 10, 2559, 2016.

Harpold, A., and Coauthors: LiDAR derived snowpack data sets from mixed conifer forests across the Western United States. Water Resour. Res., 50, 2749-2755, 2014.

Hopkinson, C., Chasmer, L., Young-Pow, C., and Treitz, P.: Assessing forest metrics with a ground-based scanning lidar. Can. J. For. Res., 34, 573-583, 2004.

470 Keyetieu, R., and Seube, N.: Automatic Data Selection and Boresight Adjustment of lidar Systems. Remote Sensing, 11, 1087, 2019.

Kirchner, P., Bales, R., Molotch, N., Flanagan, J., and Guo, Q.: LiDAR measurement of seasonal snow accumulation along an elevation gradient in the southern Sierra Nevada, California. Hydrol. Earth Syst. Sci., 18, 4261-4275, 2014.

Kraus, K., and Pfeifer, N.: Advanced DTM generation from LiDAR data. International Archives of Photogrammetry,
475   Remote Sensing and Spatial Information Sciences, 34, 23–30, 2011.

Kumari, P., Carter, W. E., & Shrestha, R. L.: Adjustment of systematic errors in ALS data through surface matching. Adv. Space Res., 47(10), 1851-1864, 2011.

Li, Z., Tan, J., & Liu, H.: Rigorous boresight self-calibration of mobile and UAV LiDAR scanning systems by strip adjustment. Remote Sens., 11(4), 442, 2019.

480 López-Moreno, J. I., Revuelto, J., Alonso-González, E., Sanmiguel-Vallelado, A., Fassnacht, S. R., Deems, J., and Morán-Tejeda, E.: Using very long-range terrestrial laser scanner to analyze the temporal consistency of the snowpack distribution in a high mountain environment. J. Mt. Sci., 14, 823-842, 2017.

Maas, H. G.: Least-squares matching with airborne laserscanning data in a TIN structure. International Archives of Photogrammetry and Remote Sensing, 33(B3/1; PART 3), 548-555, 2000.

485 Mazzotti, G., Currier, W. R., Deems, J. S., Pflug, J. M., Lundquist, J. D., and Jonas, T.: Revisiting snow cover variability and canopy structure within forest stands: insights from airborne lidar data. Water Resour. Res., 55, 6198-6216, 2019.

Meyer, J., and Skiles, S. M.: Assessing the ability of structure from motion to map high resolution snow surface elevations in complex terrain: A case study from Senator Beck Basin, CO. Water Resour. Res., 55, 6596-6605, 2019.

Monson, R. K., Lipson, D. L., Burns, S. P., Turnipseed, A. A., Delany, A. C., Williams, M. W., and Schmidt, S. K.: Winter
490   forest soil respiration controlled by climate and microbial community composition. Nature, 439, 711, 2006.

Mott, R., Schirmer, M., and Lehning, M.: Scaling properties of wind and snow depth distribution in an Alpine catchment. J. Geophys. Res.-Atmos., 116, 2011.

Mott, R., Vionnet, V., and Grünewald, T.: The seasonal snow cover dynamics: review on wind-driven coupling processes. Front. Earth Sci., 6, 197, 2018.

495 Muir, J., Goodwin, N., Armston, J., Phinn, S., and Scarth, P.: An accuracy assessment of derived digital elevation models from terrestrial laser scanning in a sub-tropical forested environment. Remote Sens., 9, 843, 2017.

Nolan, M., Larsen, C., and Sturm, M.: Mapping snow-depth from manned-aircraft on landscape scales at centimeter resolution using Structure-from-Motion photogrammetry. The Cryosphere, 9, 1445–1463, 2015.

Painter, T. H., Berisford, D. F., Boardman, J. W., Bormann, K. J., Deems, J. S., Gehrke, F., Hedrick, A., Joyce, M., Laidlaw,
500   R., Marks, D. and Mattmann, C.: The Airborne Snow Observatory: Fusion of scanning lidar, imaging spectrometer, and physically-based modeling for mapping snow water equivalent and snow albedo. Remote Sensing of Environment, 184, 139-152, 2016.

Palace, M., Sullivan, F. B., Ducey, M., & Herrick, C.: Estimating tropical forest structure using a terrestrial lidar. PLoS One, 11(4), 2016.

505 Perron, C.J., Bennett, K., & Lee, T.D.: Forest stewardship plan: Thompson farm. NH: University of New Hampshire. Produced by Ossipee Mountain Land Company, West Ossipee, https://colsa.unh.edu/sites/default/files/thompson-farm-plan.pdf, 2004.

Reinmann, A. B., and Templer, P. H.: Increased soil respiration in response to experimentally reduced snow cover and increased soil freezing in a temperate deciduous forest. Biogeochemistry, 140, 359-371, 2018.

510 Schweizer, J., Jamieson, J. B., and Schneebeli, M.: Snow avalanche formation. Rev. Geophys., 41, 25, 2003. Starkloff, T., Stolte, J., Hessel, R., and Ritsema, C.: Investigating the development of shallow snowpacks on arable land, using comprehensive field observations and spatially distributed snow modelling. Hydrol. Res., 49, 41-59, 2017.

Sturm, M., and Holmgren, J.: An automatic snow depth probe for field validation campaigns. Water Resour. Res., 54, 9695-9701, 2018.

515 Team, R. C.: R: A language and environment for statistical computing; 2018.

Tonkin, T. N., and Midgley, N. G.: Ground-Control Networks for Image Based Surface Reconstruction: An Investigation of Optimum Survey Designs Using UAV Derived Imagery and Structure-from-Motion Photogrammetry. Remote Sens., 8, 8, 2016.

Tucker, C. L., Tamang, S., Pendall, E., and Ogle, K.: Shallow snowpack inhibits soil respiration in sagebrush steppe through
520   multiple biotic and abiotic mechanisms. Ecosphere, 7, e01297, 2016.

Tuttle, S. E., Cho, E., Restrepo, P. J., Jia, X., Vuyovich, C. M., Cosh, M. H., & Jacobs, J. M.: Remote sensing of drivers of spring snowmelt flooding in the north central US. In V. Lakshmi (Ed.), Remote Sensing of Hydrological Extremes (pp. 21–45). Switzerland: Springer International Publishing. https://doi.org/10.1007/978-3-319-43744-6_2, 2017.

Vander Jagt, B., Lucieer, A., Wallace, L., Turner, D., and Durand, M.: Snow depth retrieval with UAS using photogrammetric techniques. Geosci., 5(3), 264-285, 2015.

Wallace, L., Lucieer, A., and Watson, C. S.: Evaluating tree detection and segmentation routines on very high resolution UAV LiDAR data. IEEE T. Geosci. Remote, 52, 7619-7628, 2014.

Wallace, L., Lucieer, A., Watson, C., and Turner, D.: Development of a UAV-LiDAR system with application to forest inventory. Remote Sens., 4, 1519-1543, 2012.

Watanabe, K., and Osada, Y.: Comparison of hydraulic conductivity in frozen saturated and unfrozen unsaturated soils. Vadose Zone J., 15, 2016.

Wever, N., Jonas, T., Fierz, C., and Lehning, M.: Model simulations of the modulating effect of the snow cover in a rain-on-snow event. Hydrol. Earth Syst. Sci., 18, 4657-4669, 2014.

Zhang, K., Chen, S.-C., Whitman, D., Shyu, M.-L., Yan, J., and Zhang, C.: A progressive morphological filter for removing nonground measurements from airborne LIDAR data. IEEE T. Geosci. Remote, 41, 872-882, 2003.

Zhang, Z., Sun, L., Zhong, R., Chen, D., Xu, Z., Wang, C., ... & Li, R.: 3-D deep feature construction for mobile laser scanning point cloud registration. IEEE Geosci. Remote S., 16(12), 1904-1908, 2019.